Supplementary Information

Flexible tissue-carbon nanocoils-carbon nanotubes-based humidity sensor with high performance and durability

*Chengwei Li[a], Yifeng Zhang[a], Shuaitao Yang[a], Huitong Zhao[b], Yuan Guo[a], Tianze Cong[a], Hui Huang[a], Zeng Fan[a], Hongwei Liang[b], Lujun Pan[a, *]*

[a]School of Physics, Dalian University of Technology, No. 2 Linggong Road, Ganjingzi District, Dalian 116024, P. R. China.

[b]School of Microelectronics, Dalian University of Technology, Dalian, Liaoning 116024, P. R. China.

[*]Corresponding author. E-mail: lpan@dlut.edu.cn

1. The SEM observation of tissue-CNCs-CNTs composite with different mass ratios

Figure S1 shows the SEM observation of tissue-CNCs-CNTs composite with different mass ratios of CNCs and CNTs, *i.e.*, 1:1, 1:2, 1:4, 1:8. It can be seen that with the increase of the mass proportion of CNTs, the space between the tissue fibers is gradually filled. Moreover, the number of porous structures of tissue itself and the porous skeleton structures built by CNCs on the surface of tissue decreases.

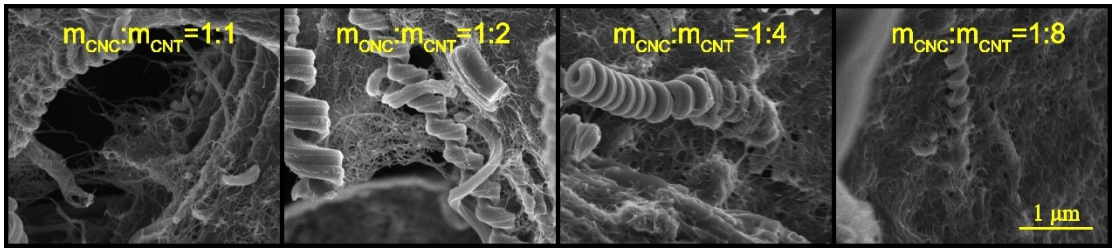

Figure S1. The SEM observation of tissue-CNCs-CNTs composite with different mass ratios of CNCs and CNTs.

2. The SEM observation of tissue-CNCs-CNTs composite with same mass ratio and different initial resistance

Figure S2 shows the SEM observation of tissue-CNCs-CNTs composite with different initial resistance. Under the premise that the mass ratio of CNCs and CNTs is 1:2, with the increase of the initial resistance, the tissue-CNCs-CNTs composite becomes more and more porous, and more and more spaces exist among tissue fibers, CNCs and CNTs. When the initial resistance is small, the composite structure becomes very dense, the surface of tissue fibers and CNCs are filled with a large amount of CNTs.

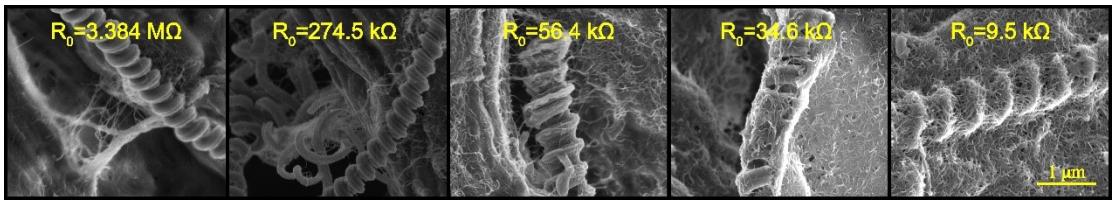

Figure S2. The SEM observation of tissue-CNCs-CNTs composite with different initial resistance under the same ratio of CNCs and CNTs.

3. The FTIR spectroscopy of the tissue paper

Figure S3 shows the FTIR spectroscopy of the tissue paper. Due to the presence of many hydrophilic hydroxyl groups on the surface of the tissue fibers, the tissue paper exhibits excellent hydrophilicity.

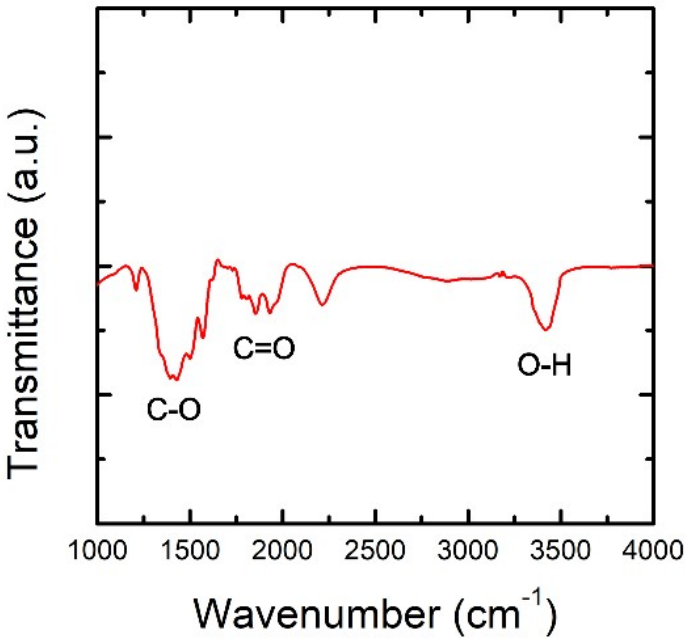

Figure S3. The FTIR spectroscopy of the tissue paper.

4. The comparison between the tubular model and slit-like model in MD simulation

Figure S4 shows the comparison between the tubular model and slit-like model in MD simulation. Modeling the pores which can be perfectly compared with experimental structure is a long puzzle, and the simplification is a common method when modeling pores. It is found that two simplified models are usually constructed as pores and can be used to store water molecules and ions. One is the slit-like pore constructed by two single layer graphene as shown in Figure S4a.[1-3] The other is the tube-like pore as shown in Figure S4b.[4] Here, we construct concentric tubes to simulate the pore structures composed of CNCs and CNTs with different addition ratios. The concentric tube is not a pore, but pores with many different sizes, reflecting the state of connection between CNCs, CNTs and tissue fibers.

Comparing with slit-like pore, the tube-like pore constructed here still maintains the boundary of sp2 carbon. Moreover, in order to calculate the density variation of water molecules based on different addition ratios of CNCs and CNTs, the pores should not be slits, but tubes with confined space. The role of pores in this paper is focused on the distribution of water in the confined space. Therefore, the tubular model is a suitable model compared with the experimental structure of pores.

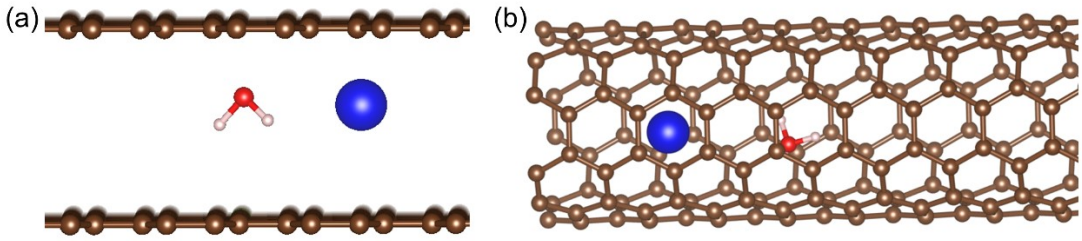

Figure S4. (a) Schematic illustration of the slit-like pore with water and ions. (b) The model of tube-like pore in our work.

5. The DFT calculations for p-type models

In this paper, the porous models are based on sp^2 CNT. Therefore, we use the B-doped graphene-water interface to represent the sp^2 polar interface of the p-type model. The charge transfer is reflected in charge differential density (**Figure S5**a), and the mixing of $3a_1$ orbital shown in density of state (DOS) determines the water geometry sitting on the surface with oxygen pointing to surface and hydrogen slightly tilting up, indicating the electron interaction in Figure S5b. It is illustrated that this is a very local phenomenon. However, the experiential results are deeply based on the distribution of overall water molecules in the pore.

Based on the above analysis and the illustration in Figure S5, the p-type behavior only affects the adsorption behavior of water in the local polar regions through the mixing of $3a_1$ orbit, and the fixed repulsion of water in the local regions remains at 3 Å. However, this paper focus on the effect of different addition ratio and amount of CNCs and CNTs on the overall water density of the system. Considering the size of pores and the dynamic characteristics of the water molecules, we chose the traditional MD simulation method and ignored the p-type behavior which has little influence on the calculation result.

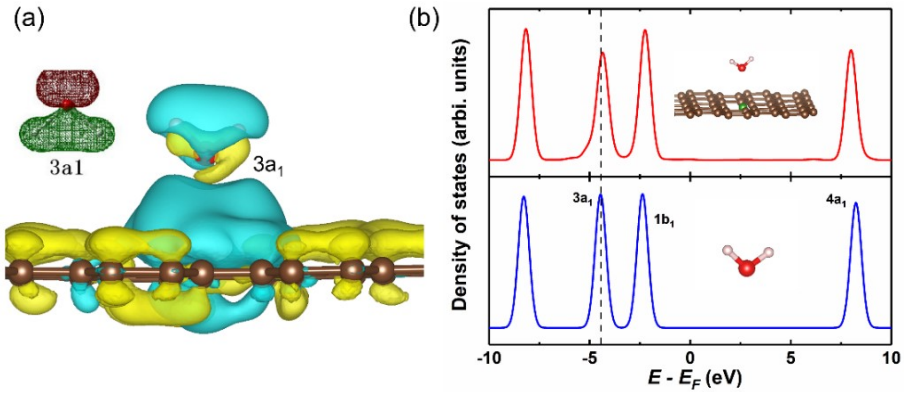

Figure S5. (a) Charge differential density of B-graphene/water interface. (b) Projected DOS plots of water molecules in interface and bulk region.

6. The reproducibility of the sensors based on tissue-CNCs-CNTs

In order to evaluate the reproducibility of the humidity sensors based on tissue-CNCs-CNTs. Five sensors with the same fabrication parameters, *i.e.*, addition ratio of m_{CNC}:m_{CNT}=1:2, effective sensing area of 2 cm × 1 cm and initial resistance between 260 to 280 kΩ, were fabricated. Their humidity sensing performances were tested in the relative humidity range of 10-90% respectively, as shown in **Figure S6**. It is obvious that the resistance response ($\Delta R/R_0$) and the sensitivity are 4.93±0.14 and (6.17%±0.18%)/% RH, respectively. The deviations are less than 3%, indicating an excellent reproducibility of the humidity sensor.

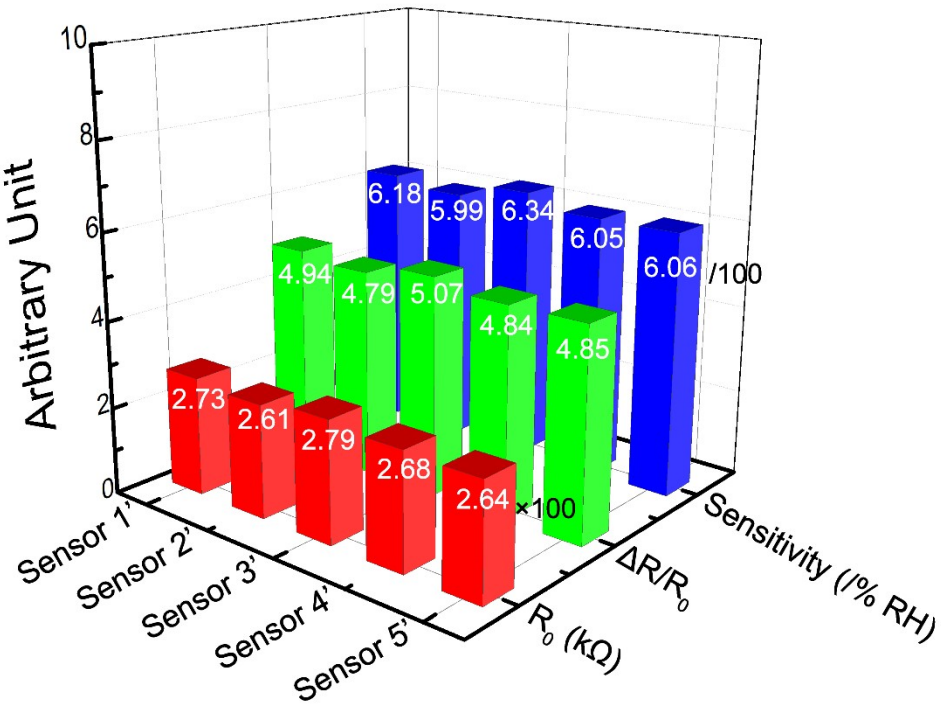

Figure S6. The reproducibility of the sensors based on tissue-CNCs-CNTs.

References

1. R. Futamura, T. Iiyama, Y. Takasaki, Y. Gogotsi, M. J. Biggs, M. Salanne, J. Segalini, P. Simon and K. Kaneko, *Nat Mater*, 2017, **16**, 1225-1232.
2. S. Kondrat and A. Kornyshev, *J Phys-Condens Mat*, 2011, **23**, 022201.
3. J. Vatamanu, M. Vatamanu and D. Bedrov, *Acs Nano*, 2015, **9**, 5999-6017.
4. H. Shao, Y. C. Wu, Z. F. Lin, P. L. Taberna and P. Simon, *Chem Soc Rev*, 2020, **49**, 3005-3039.